Journal of The Electrochemical Society, **146** (1) 339-349 (1999)
S0013-4651(98)01-009-X CCC: $7.00 © The Electrochemical Society, Inc.

Characterization of a Time Multiplexed Inductively Coupled Plasma Etcher

A. A. Ayón,* R. Braff, C. C. Lin, H. H. Sawin,* and M. A. Schmidt*

Microsystems Technology Laboratories, Massachusetts Institute of Technology, Cambridge, Massachusetts 02139, USA

We report the experimentally obtained response surfaces of silicon etching rate, aspect ratio dependent etching (ARDE), photoresist etching rate, and anisotropy parameter in a time multiplexed inductively coupled plasma etcher. The data were collected while varying eight etching variables. The relevance of electrode power, pressure, and gas flow rates is presented and has been found to agree with observations reported in the literature. The observed behavior presented in this report serves as a tool to locate and optimize operating conditions to etch high aspect ratio structures. The performance of this deep reactive ion etcher allows the tailoring of silicon etching rates in excess of 4 μm/min with anisotropic profiles, nonuniformities of less than 4% across the wafer, and ARDE control with a depth variation of less than 1 μm for trenches of dissimilar width. Furthermore it is possible to prescribe the slope of etched trenches from positive to reentrant.

Manuscript submitted January 6, 1998; revised manuscript received July 13, 1998.

The development of silicon processing has been characterized by the aim to miniaturize structures and to fabricate faster devices. This is clearly illustrated, for example, by the fact that the number of components per integrated circuit rose from a few thousands in the early 1960s to millions in the 1990s. This dramatic trend has been possible due to advances in a wide range of microfabrication technologies and materials, including the understanding of plasma etching phenomena and the availability of silicon processing equipment with improved etching capabilities. The bonanza in research and production of silicon-based devices has also stimulated the growth of certain fabrication approaches such as microelectromechanical systems (MEMS).

MEMS combine miniaturization, sensing or actuating behavior, and electronic interfacing to fabricate devices for a large variety of applications. Pressure sensors, accelerometers, microchemical reactors, gyroscopes, and micromirror displays are but a few examples of the structures found in MEMS.

Some MEMS devices also involve high aspect ratio structures (HARS) which permit the fabrication of devices able to span from 0.1 to 1 mm, and that are compliant in the plane of the wafer but rigid in the direction normal to its surface.[1] HARS also permits achieving large lateral capacitances. HARS in combination with other technologies, such as wafer bonding, also make possible the realization of novel and promising applications, such as power MEMS.[2]

Among the options for fabricating HARS in silicon, we find reactive ion etching (RIE) and electron cyclotron resonance (ECR). However, these conventional dry processing approaches have only had a limited success in fulfilling the requirements of HARS: high etch rate, good selectivity to masking material, anisotropy, and compatibility with other processes.[3] Both RIE and ECR permit anisotropic profiles but the etching rate is usually low and etching beyond a few dozens of microns is time consuming. Furthermore, the selectivity even to hard masks like silicon dioxide usually does not exceed 20:1.

Another alternative for fabricating HARS is the lithography-electroplating-injection-molding (LIGA, German acronym)[4] process. LIGA offers the largest anisotropy achievable in micromachined structures, and excellent profile control, at the expense of requiring a synchrotron radiation source and limited compatibility with other processes. Thus, a significant research effort has been made to develop a LIGA-like process which would not require an X-ray source. A solution has been found with high density plasma tools which combine the ability to fabricate HARS with results comparable to LIGA but with a technology similar to the well-known RIE.

In particular, inductively coupled plasmas (ICP) are satisfying the need of the aforementioned processes, and the purpose of this article is to present the measured results of one of these tools. ICP etchers provide high concentrations of etching species at low pressures and low dc bias. It is the ionization efficiency of ICP that has made it a valuable tool not only for etching applications but also for mass spectrometry.[5] However, when applying a fluorinated gas, such as SF_6, the nature of the etch is isotropic[6] due to the spontaneous silicon etching rate of fluorine,[7,8] and the high volatility of the products. Sidewall passivation steps must be performed to improve the anisotropy of the etch.[9-10] The technique patented by Robert Bosch GmbH[11] relies precisely on the deposition of inhibiting films to obtain anisotropic profiles. This technique is described in the following section, followed by the experimental approach. The measured performance is then presented. The responses, and their dependence on operating conditions, are silicon etching rate, photoresist etching rate, uniformity, aspect ratio dependent etching, and anisotropy.

Time Multiplexed Deep Etching

The time multiplexed deep etching (TMDE) technique developed and licensed by Robert Bosch GmbH utilizes an etching cycle flowing only SF_6 (steps b and d in Fig. 1) and then switching to a sidewall passivating cycle using only C_4F_8 (step c in Fig. 1). During the subsequent etching cycle, the passivating film is preferentially removed from the bottom of the trenches due to ion bombardment, while preventing etch of the sidewalls. The success of Bosch's TMDE scheme hinges upon the deposition of the inhibiting films. These films prevent the etching of the sidewalls by SF_6 discharges that contain large concentrations of atomic fluorine which spontaneously etches silicon. SF_6 discharges lack polymer-forming species to block spontaneous etching.[12,13] However, fluorocarbon discharges contain a variety of radicals[14,15] that form Teflon-like films on all surfaces. This is also consistent with reports of C_4F_8 having characteristics equivalent to those of CF_4 with a suitable amount of CH_4 added.[16]

The duration of etching and passivating cycles, applied electrode and coil powers, and gas flow rates can each be prescribed independently. However, as can be seen in Fig. 2, there is always a gas flow overlap, of around 1 s, due to the finite time response of the mass flow controllers. This overlap can be extended even more by prescribing an additional time overlap at the end of either or both cycles.

The Bosch technique uses the high etching rate of a fluorine-rich plasma to etch HARS. Even etching through the wafer is feasible. Some recently reported applications are already exploiting this latter alternative.[17-19] Furthermore, by suppressing the time multiplexing, the equipment can be run with continuous flows of SF_6 or C_4F_8. With SF_6 it is possible to achieve isotropic etch rates as high as 8.28 μm/min. Using C_4F_8, Teflon-like films can be deposited for use as antistiction films.[20] Soft lithography being a process which involves transfer molding of organic polymers,[21] can benefit from the ability to in situ deposit of Teflon-like films, as release layers.

* Electrochemical Society Active Member.

S0013-4651(98)01-009-X CCC: $7.00

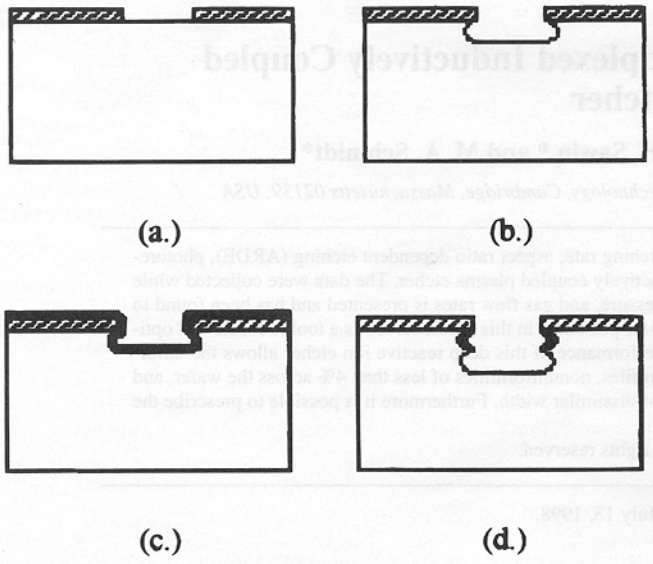

Figure 1. TMDE scheme: (a) Patterned photoresist mask on a silicon wafer, (b) etching cycle, the isotropic nature of the etch is clearly identifiable, (c) during the passivation cycle a Teflon-like film is deposited on all surfaces, and (d) during the subsequent etching cycle, the thin passivating film is first removed from all surfaces exposed to ion bombardment and then the etch proceeds. Once more the isotropic nature of the etch is clearly shown.

The large parameter space for the etch system has proven to be versatile enough to allow prescribing the profile of the etched features as well as surface roughness and selectivity.

Experimental

This work was performed using a Surface Technology Systems multiplex ICP (Redwood City, CA). Vacuum pumping of the etching chamber is done by a Balzers TMH1000C (Pfeiffer Vacuum Technologies, Hudson, NH) turbopump, with a pumping speed of 880 L/s.

The equipment includes two independent 13.56 MHz rf power sources: a 1000 W supply for the single-turn coil around the etching chamber to create the plasma and a 300 W supply connected to the wafer electrode to vary the rf bias potential of the wafer with respect to the plasma. The efficient inductive power coupling of the coil to the plasma allows high density plasmas to be maintained. This coil is connected between the matching network and ground. The phase between the rf power sources is optimized with a linear-phase shift controller.

The etching and passivating gases enter from the top of the etching chamber, through a single gas feed located 7 cm off-center. The gases are then routed through a series of grooves on the top cover intended to distribute them evenly across the wafer. Finally, the gases access the chamber through a 2.9 mm groove of diameter 103 mm located on top of the wafer. The gas is pumped through a single large opening located opposite to the load lock gate (see Fig. 3).

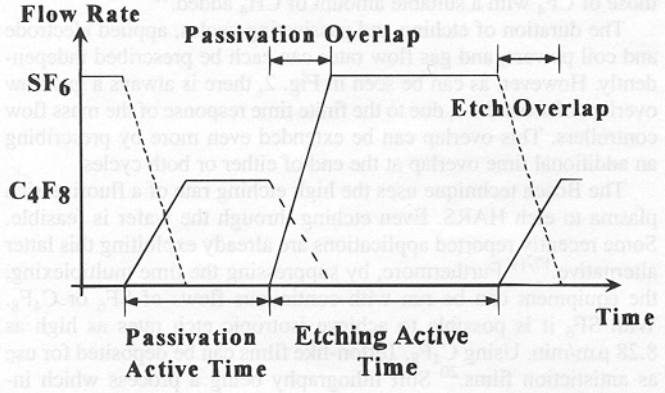

Figure 2. Graph showing the gas flow cycles during plasma etching. Note the overlaps caused by the finite time response of the mass flow controllers.

Back-side helium pressurization is used to provide good heat transfer between the wafer and the electrode to maintain a constant wafer temperature. A set of eight alumina fingers, with interfinger distance of 89.9 mm, clamp the wafer to the electrode (see Fig. 3). Additionally, an elastomer in the electrode creates a seal to avoid helium leaks while etching. The measured temperature on the surface of the wafer during processing is 40°C. These low temperatures reduce the etching rate of the photoresist, thereby allowing its use as a mask for etching silicon. Photoresist can also be used as a bonding material for mounting the device wafer to a handle wafer during processes requiring etching through a wafer. This mounting is required to prevent helium leaks into the chamber. For very small features, device wafers can be mounted on quartz for visual detection of the etch completion. The top cover of the etching chamber is water heated and maintained at 40°C.

It is possible to operate with a predetermined common pressure for both etching and passivating active cycles, or with a fixed angular position for the automatic pressure control valve (APC). In the first case the position of the throttle valve (or APC valve) varies as the gas flow changes during each cycle. In the latter case, the position of the throttle valve is fixed and the pressure is determined by the gas flow rate. The results presented in this report used this latter approach. Higher values of the APC valve position in degrees correspond to higher pressures. However, the trip pressure is fixed at 90 mT creating an upper limit in these experiments. Tables I and II present the measured pressure under static conditions for both gases as well as the corresponding residence times.

The residence time, τ, is proportional to pV/f, where p is the pressure, V is the chamber volume, and f is the gas flow rate. This time is important in relation to the removal rate of etch products in the process chamber with the corresponding effect on reactant concentration.[22] Thus, high APC settings or low flow rate (see Tables I and II) can both have deleterious effects on etching characteristics.

Eight variables were studied in this experiment, namely, SF_6 flow rate, etching active time or etching cycle, etch overlap, electrode

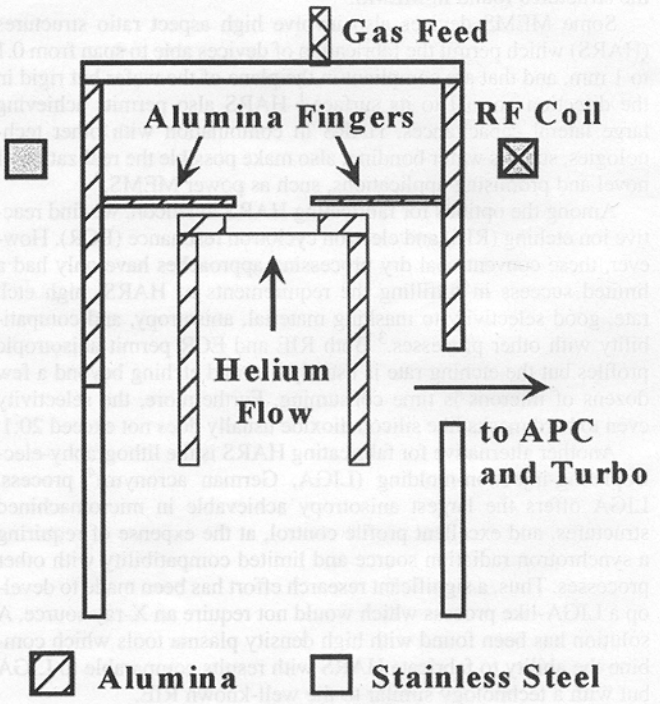

Figure 3. General sketch of the etching chamber (not to scale) with volume of 36 L. The gas feed is located 7 cm off the center of the upper cover. After being routed through an array of grooves the corresponding gases enter the etching chamber through a single continuous shower groove with outer diameter 103 mm and width 2.9 mm.

S0013-4651(98)01-009-X CCC: $7.00 © The Electrochemical Society, Inc.

Table I. Steady-state pressure vs. SF_6 flow rate.

APC (°)	SF_6 flow rate (sccm)	Pressure (mT)	Residence time (s)
50	70	6.6	0.27
50	140	11.4	0.23
65	70	13.8	0.56
65	140	24	0.49
80	70	60.8	2.47
78	140	85	1.73

Table II. Steady-state pressure vs. C_4F_8 flow rate.

APC (°)	C_4F_8 flow rate (sccm)	Pressure (mT)	Residence time (s)
50	20	2.2	0.31
50	95	8.4	0.25
65	20	4.6	0.65
65	95	18	0.54
80	20	26.3	3.74
80	95	85	2.54

power during etching, C_4F_8 flow rate, passivation active time or passivating cycle, electrode power during passivation, and APC position in degrees.

The default passivation overlap over the etching cycle was not modified, and the inductive coil power was fixed at 600 W during both etching and passivating cycles. Etches were performed for 30 min to study etch rate, ARDE, and anisotropy. Additional 5 min etches were performed to determine photoresist removal rate and uniformity.

For the 30 min runs the samples were prepared in the following fashion: 4 in. single-crystal silicon <100> wafers, n-type with resistivity between 6 and 20 Ω cm, were coated with photoresist AZ4620 spun at 3000 rpm (thickness ≈ 6 μm) and baked in a convection oven at 90°C for 30 min. The samples were then exposed in a contact Karl Suss aligner with a wavelength of 320 nm and power density of 6 mW/cm^2, developed with AZ440, and baked again at 90°C for 30 min. The mask consists of arrays of trenches of widths of 2 to

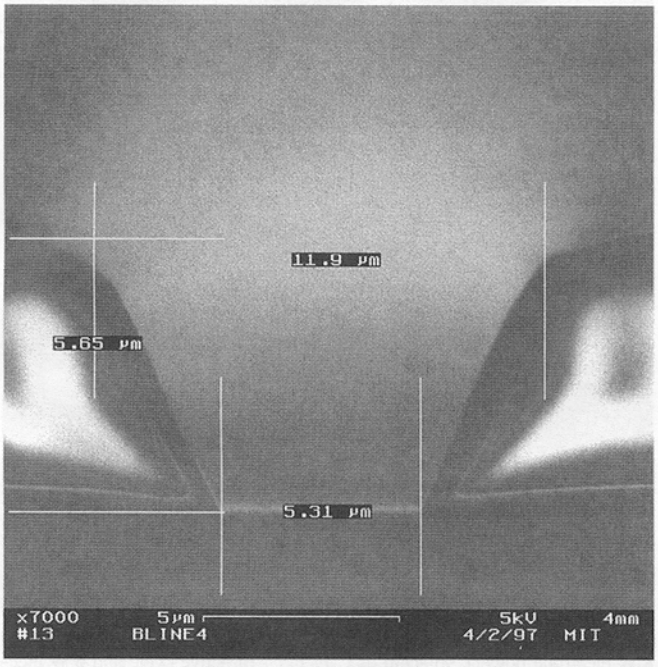

Figure 4. Micrograph showing the profile of the photoresist used as a mask for the 30 min etches.

Table III. Range of explored variables.

Variable	Minimum	Maximum
SF_6 flow rate	70 sccm	140 sccm
SF_6 active time	10 s	15 s
Etch overlap	0	1 s
Electrode power during etch	8 W	16 W
C_4F_8 flow rate	20 sccm	95 sccm
C_4F_8 active time	6 s	11 s
Electrode power during passivation	0	6 W
APC	50°	80°

64 μm, that expose a wafer area of 18%. The photoresist profile is not anisotropic as can be seen in Fig. 4. After etching the samples, we used SEM to study them.

For the 5 min runs we used photoresist OCG 825 (20 cs) spun, baked, and exposed in the same fashion but developed with OCG 934 (1:1). In this case the expected photomasking material thickness is approximately 1 μm. We used an optical interferometer to measure the thickness of the photoresist layer before and immediately after etching each sample, and a profilometer to measure the depth of the etched trenches. No noticeable difference in photoresist etching rate was detected between AZ4620 and OCG825.

Once the samples were prepared, a designed set of experiments adequate to fit a quadratic model were performed and analyzed using commercial software. The explored ranges are presented in Table III. This systematic investigation produced response surfaces[23-25] that enable us to predict appropriate operating conditions for different processing requirements.

Results

The measured etching rate, ARDE, uniformity, photoresist etching rate, and anisotropy parameter were fitted and the corresponding response surfaces generated. The relevant dimensions are introduced in Fig. 5, and they are defined in the respective sections for each response.

Flow rate, pressure, and applied power, are the dominant variables that determine the etching characteristics. Pressure, for in-

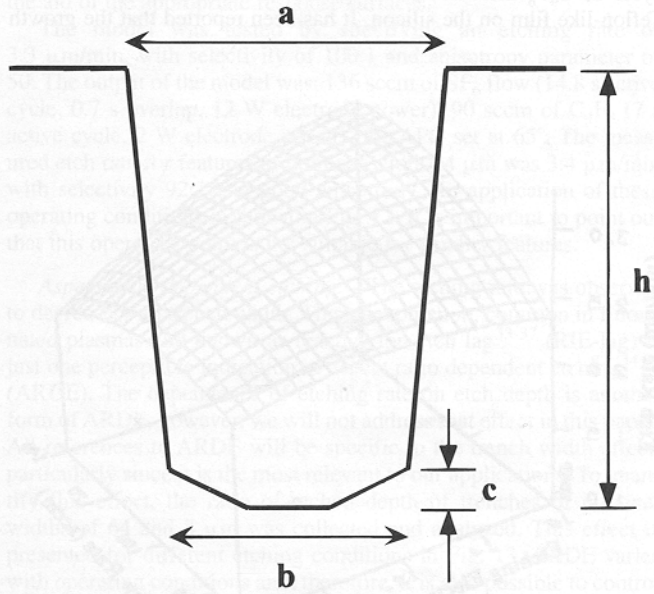

Figure 5. Drawing showing the main dimensions used in this report. The mask thickness is not included. Silicon etching rate is obtained by dividing the depth achieved, h, by the etching time. Selectivity is the ratio of silicon depth attained, h, to the photoresist removed. The anisotropy parameter is defined as $(h\text{-}c)/|a\text{-}b|$.

S0013-4651(98)01-009-X CCC: $7.00 © The Electrochemical Society, Inc.

stance, increases the formation of atomic fluorine and other radicals, relative to that of ions, and, thus, promotes isotropic profiles. It also reduces the maximum ion energy, the sheath width, and the bias drop across the electrode sheath.[24,26,27] Applied electrode power increases the self-bias and the ion directionality and hence etching anisotropy. Ion bombardment energy increases typically increase the etching rate of the photoresist relative to that of silicon, thereby decreasing the selectivity.[28,29] Finally, increasing the flow rate increases the removal rate of etching products and significantly effects the etching rate.[30] Hence etching rate, etch selectivity, anisotropy, and uniformity all have a noticeable dependence on pressure, applied power, and flow rates.

All response contours were generated holding the variables not explored in each figure at a value corresponding to the middle point of their explored range (see Table III).

Silicon etching rate.—Figures 6 and 7 show the etching rate variation as a function of operating conditions. The average etching rate is defined as the ratio of the total depth, h, divided by the etch time (30 min). All measurements graphed in Fig. 6 and 7 were taken for trenches of nominal width, 64 μm. The adjusted R^2 of the quadratic model for this response is 0.85 indicating that the fit is reasonably good.[25]

The etching rate of silicon has three components: physical sputtering, spontaneous thermal etching, and ion-enhanced chemical reaction; the largest component being the ion-enhanced part.[22] Thus, increases in applied electrode power during the etching cycle represent additional gas ionization, dissociation,[27] and, more importantly, additional ion bombardment energy which is reflected in higher etch rates (see Fig. 6). For low SF_6 flows, power increases only have a marginal effect on etching rate. At low flows the concentration of etchant (F) is limited and the concentrations of products (SiF_4) that redeposit increases.[30]

As the flow rate increases, the etching rate increases with both flow rate and applied electrode power.[31]

The etching rate dependence on pressure is shown in Fig. 7. The etching rate initially increases with pressure due to higher F concentrations,[22,26] but as pressure is increased even further, the ion energy and/or flux is reduced and the etching rate drops.[22]

The etching rate also increases as the etching active cycle duration is increased due to greater fractional etching times with SF_6. Similarly, the etching rate decreases as the duration of the active cycle of C_4F_8 increases (see Fig. 7) due to thicker depositions of Teflon-like film on the silicon. It has been reported that the growth

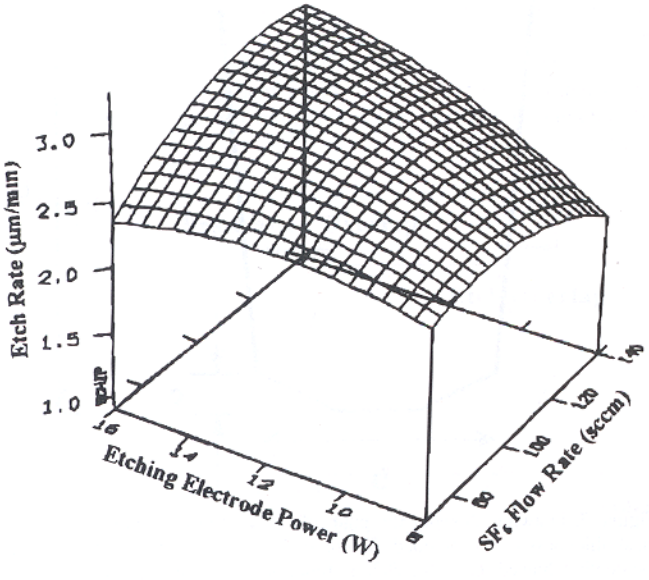

Figure 6. Silicon etching rate as a function of SF_6 flow rate and applied electrode power during the etching cycle.

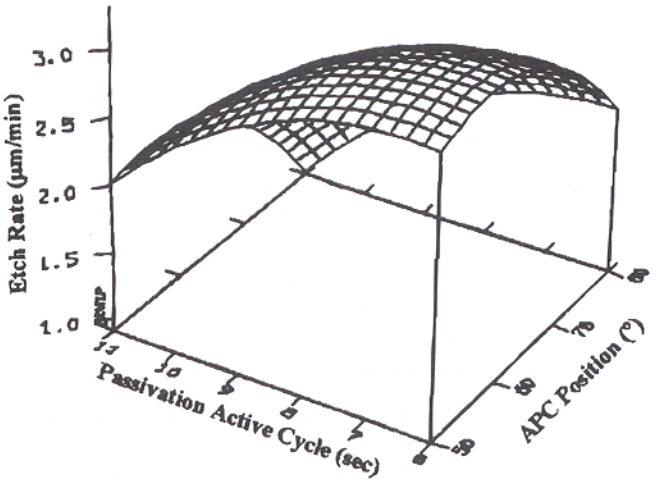

Figure 7. Silicon etching rate as a function of APC position (pressure) and passivation cycle duration.

of the fluorocarbon layer is self-limiting,[32] however, in the presence of ion bombardment, its thickness is believed to vary proportionally with deposition time. Figure 8 presents the profile of a trench etched with significant passivation depositions. The profile is anisotropic, but the average etching rate is only 1.1 μm/min.

It was also observed that silicon etching rate has only a mild dependence on C_4F_8 flow rate and applied electrode power during passivation.

The active cycle of SF_6 also determines the peak to peak height of the scalloping noticed on the walls in Fig. 9. The depth variation of the aforementioned scalloping is a function of the operating conditions and amplitudes as low as 50 nm have been detected. In general higher power to pressure ratios and shorter etching cycles tend to decrease this effect.

The active cycle overlap of SF_6 not only extends the etching time but, more importantly, reduces the flickering when switching be-

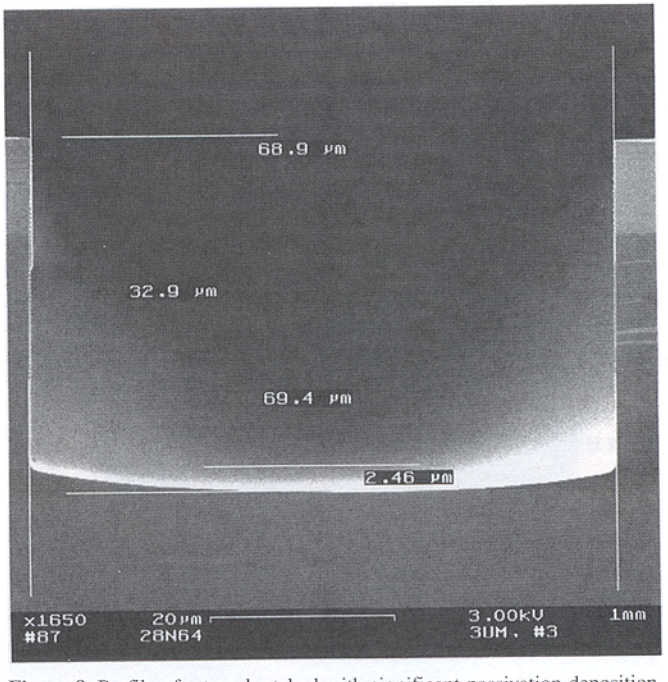

Figure 8. Profile of a trench etched with significant passivation deposition. Etching conditions were: 70 sccm of SF_6 (12.5 s active cycle, no overlap, and 8 W electrode power), 95 sccm of C_4F_8 (11 s of active cycle and 6 W electrode power), the APC set at 50°. Notice the relatively sharp corner at the trench bottom.

S0013-4651(98)01-009-X CCC: $7.00

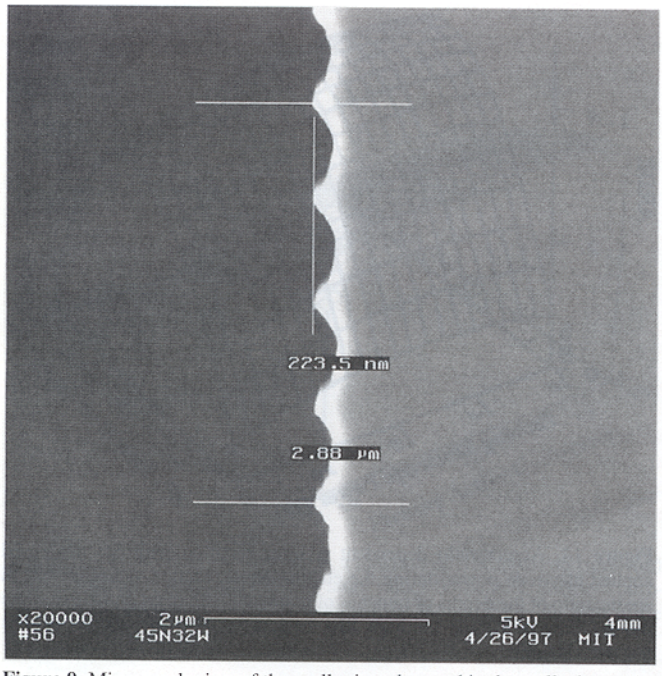

Figure 9. Micrograph view of the scalloping observed in the walls due to the periodic etch/deposition. The operating conditions were: 140 sccm of SF_6 (10 s active cycle, 1 s overlap, and 16 W electrode power), 20 sccm of C_4F_8 (11 s of active cycle and 0 W electrode power), the APC positioned at 50°.

tween an etching plasma and a passivating one. This is relevant because stable glow discharges are more amenable to uniformity and reproducibility while the currents induced by nonuniform plasmas can damage electronic devices.[15]

The large parameter space presented in this report makes the utilization of response surfaces a required tool to assess the combined effect of modifying operating conditions. This is particularly important when those changes have an opposite influence in a specific response. Figures 10 and 11 illustrate this point. In Fig. 11, the electrode power during the etching phase has been lowered from 16 to 12 W, while this power has been increased from 3 to 6 W during polymerization. The SF_6 active cycle was increased from 10 to 15 s and the SF_6 gas overlap time has been increased from 0 to 1 s. Also

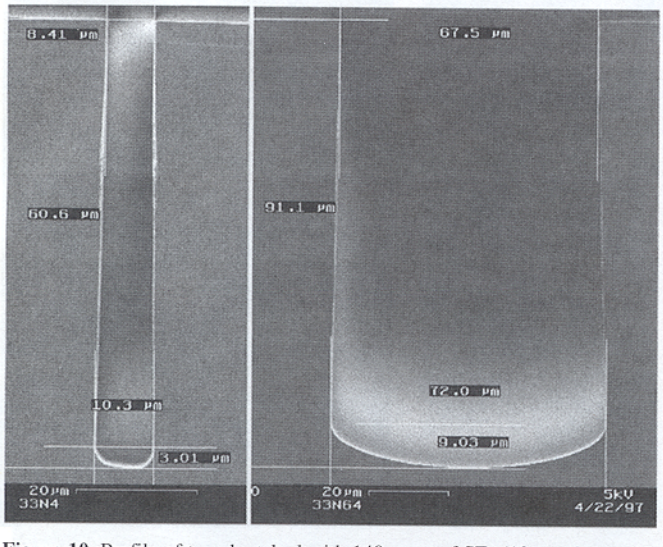

Figure 10. Profile of trench etched with 140 sccm of SF_6 (10 s active cycle, no overlap and 16 W electrode power), 20 sccm of C_4F_8 (6 s of active cycle and 3 W electrode power), the APC positioned at 65°. The anisotropy of the smaller gap is larger than that of the wider trench.

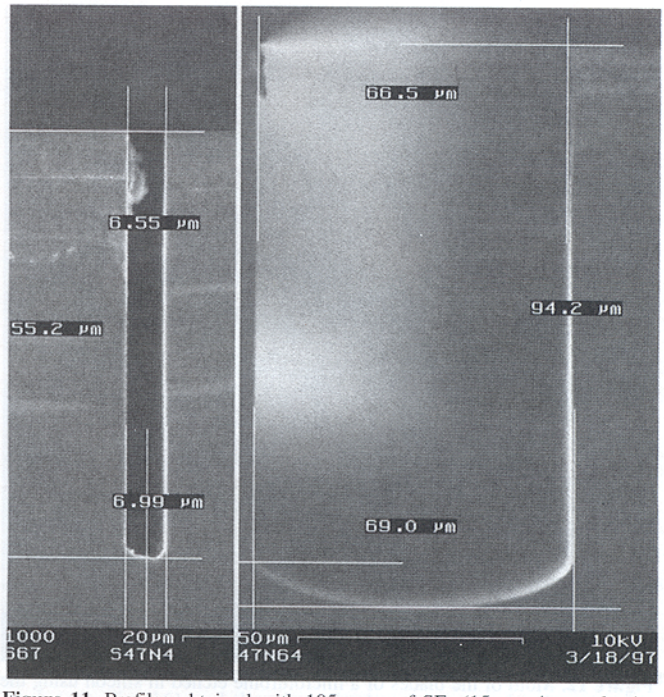

Figure 11. Profiles obtained with 105 sccm of SF_6 (15 s active cycle, 1 s overlap, and 12 W electrode power), 20 sccm of C_4F_8 (11 s of active cycle and 6 W electrode power), the APC positioned at 65°. Once more, the anisotropy of the smaller gap is larger than that of the wider trench presented in this micrographs.

the SF_6 flow rate has been decreased from 140 to 105 sccm. Finally, the polymerization cycle was increased from 6 to 11 s. The decrease in SF_6 flow rate and applied power during etching and the increase of the duration of the passivation cycle, all tend to reduce the etching rate (Fig. 6). However, the increased duration of the active cycle during etching tends to increase the etching rate (Fig. 7). Finally, as was previously mentioned, changes in applied electrode power during passivation have only a marginal influence on etching rate. With all modifications in place, the measured etching rate is only slightly affected. However, the final outcome is difficult to predict without the aid of the appropriate response surfaces.

The model was tested by specifying an etching rate of 3.3 µm/min, with selectivity of 100:1 and anisotropy parameter of 50. The output of the model was: 136 sccm of SF_6 flow (14.8 s active cycle, 0.7 s overlap, 12 W electrode power), 90 sccm of C_4F_8 (7 s active cycle, 2 W electrode power), the APC set at 65°. The measured etch rate for features of nominal width 64 µm was 3.4 µm/min with selectivity 92:1 and good anisotropy. An application of these operating conditions is shown in Fig. 12. It is important to point out that this operating point is not suitable for smaller features.

Aspect ratio dependent etching.—The etching rate was observed to decrease with trench width. This phenomenon, common in fluorinated plasmas and known as reactive ion etch lag[33-37] (RIE-lag) is just one perceptible indication of aspect ratio dependent etching[34,35] (ARDE). The dependence of etching rate on etch depth is another form of ARDE, however, we will not address that effect in this paper. All references to ARDE will be specific to the trench width effect, particularly since it is the most relevant to our applications. To quantify this effect, the ratio of etched depth of trenches of nominal widths of 64 and 8 µm was collected and analyzed. This effect is presented for different etching conditions in Fig. 13. ARDE varies with operating conditions and, therefore, it is also possible to control this behavior as is shown in the same Fig. 13.

We have found that the operating conditions required to minimize ARDE with the present fluorinated chemistry, involve high SF_6 flow rates (see Fig. 14). This observation has already been reported by other authors[33,34] and it is thought to be related to reduction of the product

Journal of The Electrochemical Society, **146** (1) 339-349 (1999)
S0013-4651(98)01-009-X CCC: $7.00

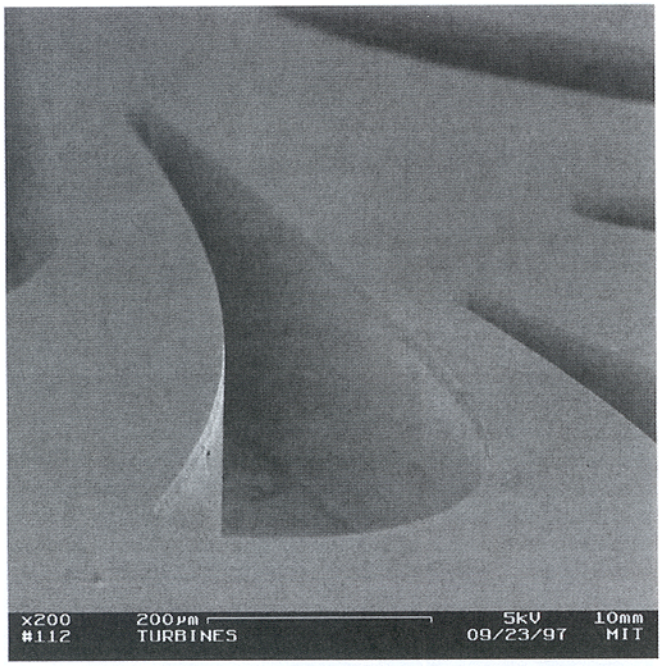

Figure 12. Mold of the blades of a microturbine etched in silicon using the output generated by the model. The depth of the trench is 180 μm.

species in the discharge which contribute to redeposition. Although the model also predicts windows of opportunity with low SF_6 flow rate regimes, that particular region has not been fully explored.

An example that exhibits small ARDE is shown in Fig. 15. Trenches of 8.16 and 35.3 μm widths achieved the same depth. However, the profile of the bottom of the trench changes from concave for a smaller trenches, to convex for trenches with widths beyond ~50 μm. If such a profile is critical in a particular application, a compromise has to be made between ARDE and the squareness of the feature bottom.

SF_6 flow rate is the dominant variable that influences the RIE lag. However, other variables have a lesser effect as shown in Fig. 14 for the applied electrode power during etching.

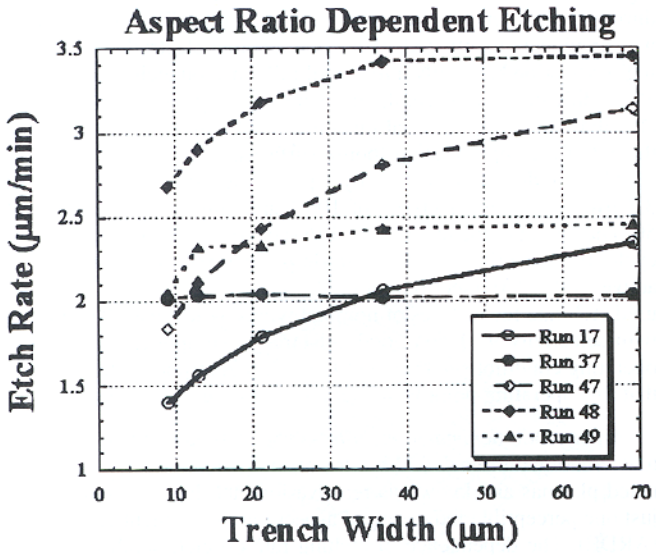

Figure 13. Aspect Ratio Dependent Etching variation with trench width. Run 17: 140 sccm of SF_6 (15 s active cycle, no overlap and 8 W electrode power), 20 sccm of C_4F_8 (11 s of active cycle and 6 W electrode power), the APC positioned at 50°. Run 37: 140 sccm of SF_6 (15 s active cycle, 0.5 s overlap, and 12 W electrode power), 95 sccm of C_4F_8 (11 s of active cycle and no electrode power), the APC positioned at 65°. Run 47: 105 sccm of SF_6 (15 s active cycle, 1 s overlap, and 12 W electrode power), 20 sccm of C_4F_8 (11 s of active cycle and 6 W electrode power), the APC positioned at 65°. Run 48: 140 sccm of SF_6 (15 s active cycle, no overlap, and 12 W electrode power), 58 sccm of C_4F_8 (6 s of active cycle and 6 W electrode power), the APC positioned at 65°. Run 49: 70 sccm of SF_6 (12.5 s active cycle, 0.5 s overlap, and 8 W electrode power), 95 sccm of C_4F_8 (6 s of active cycle and no electrode power), the APC positioned at 65°.

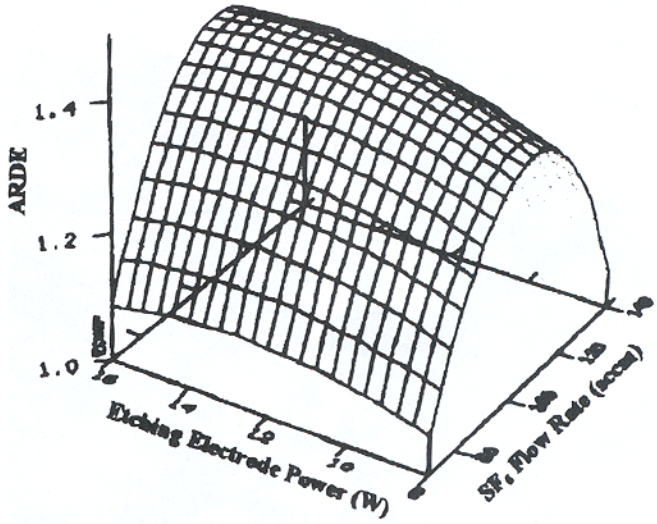

Figure 14. Aspect ratio dependent etching variation with SF_6 flow and applied electrode power during the etching phase. Plotted values of ARDE are the ratio of the depths of trenches of nominal width of 64 and 8 μm. Note the decrease of ARDE for high SF_6 flow rates. The adjusted R^2 of this response is 0.82.

Photoresist etching rate.—Low photoresist removal rate is necessary for a robust operation. Figure 16 shows the photoresist etching rate dependence on APC position and duration of the etching cycle. The removal rate is obtained by measuring the masking material thickness with an interferometer before and after etching. The adjusted R^2 for this variable is 0.90. This response is sensitive to applied electrode power, pressure, and the duration of the etching

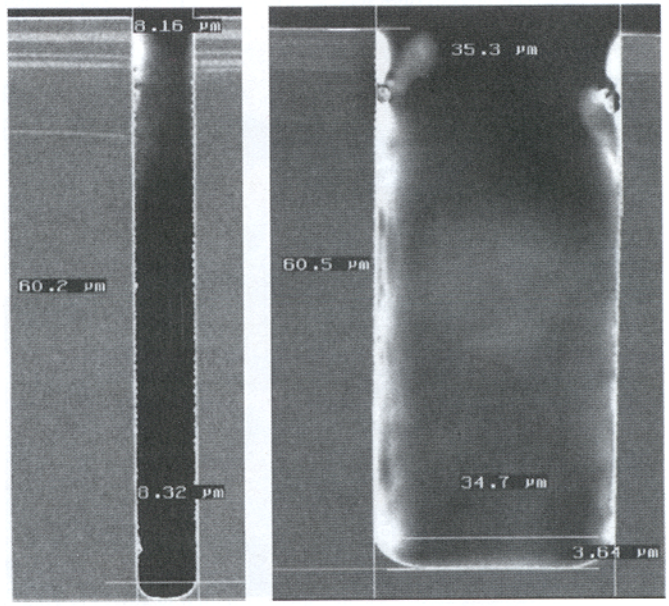

Figure 15. Trenches with openings of 8.16 μm (left) and 35.3 μm showing a depth variation of 0.3 μm after a 30 min etch. Operating conditions specified in Fig. 13 under run 37. The bottom of the trench is less concave for the wider trench. For even larger trenches, the feature bottom becomes convex.

S0013-4651(98)01-009-X CCC: $7.00 © The Electrochemical Society, Inc.

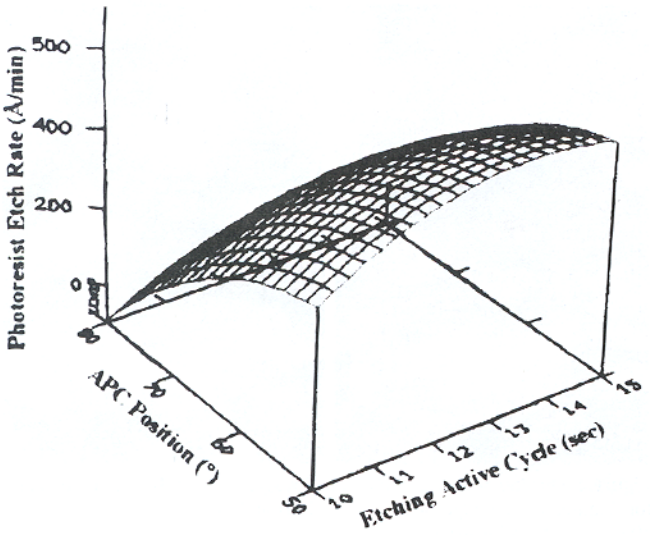

Figure 16. Photoresist etching rate as a function of APC position (pressure) and etching cycle duration. For very large values of the APC position, polymer deposition exceeds the removal during the etching cycle; the effects are usually deleterious for the profile of the etched features.

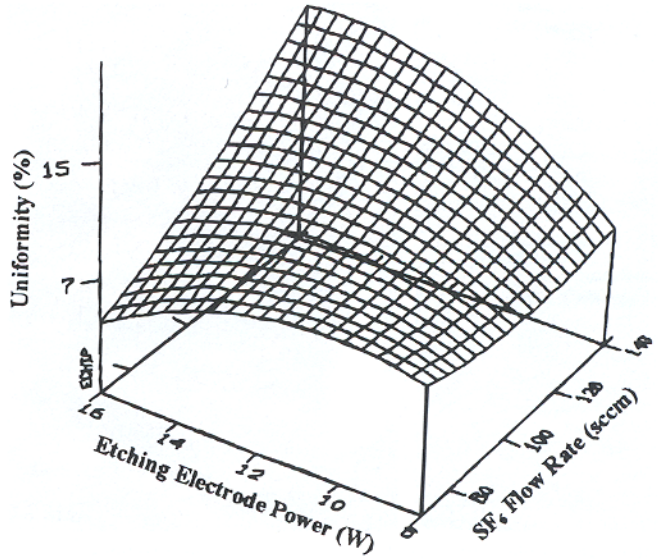

Figure 18. Uniformity dependence on SF_6 flow rate and applied electrode power during the etching cycle. The adjusted R^2 of this variable is 0.86.

and passivating cycles. The photoresist etching rate increases with applied electrode power which increases ion bombardment energy, therefore, increasing ion bombardment improves the etching anisotropy but lowers the selectivity.[39]

Although the photoresist etching rate decreases as the pressure is increased (see Fig. 16), there are several other important implications associated with large settings of the APC, namely, the sputtering and redeposition of masking material which promotes the formation of microcolumns or "grass,"[38] the damage of structures (see Fig. 17) and polymer deposition. This latter observation is represented as a negative removal rate in Fig. 16. This passivation significantly slows the etching rate and can even stop the etching of the substrate altogether. These conditions limit the range of useful settings to no more than 75°. The duration of the active etching cycle determines the exposure time of the masking material during the etch (see Fig. 16) and therefore the longer the cycle, the more the photoresist is etched. Similarly, the thickness of the polymerization film increases with time, thereby decreasing the photoresist removal rate with increasing passivation cycle time.

Uniformity.—The variation of etching rate uniformity with operating conditions is shown in Fig. 18. Plotted values were obtained by comparing the depth of trenches of nominal width of 64 μm in the middle of the wafer, with trenches located 3 cm away (Fig. 19) according to $100(1 - h/h_{middle})$. The same Fig. 19 shows the trench depth measured on a wafer after etching for 5 min as measured using a profilometer, the profiles corresponding to the operating conditions are shown in Fig. 20.

Ideally, users would avoid overetching samples if the depth of etched features across the wafer was the same. In the particular case of this ICP, nonuniformities are explained in terms of the geometric

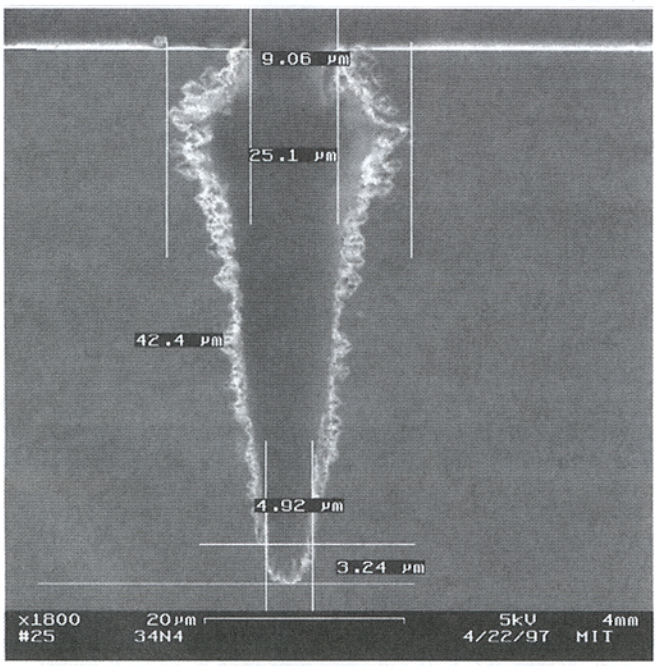

Figure 17. Profile etched with 70 sccm of SF_6 (15 s active cycle, 0.5 s overlap, and 16 W electrode power), 95 sccm of C_4F_8 (8.5 s of active cycle and 3 W electrode power), the APC positioned at 80°.

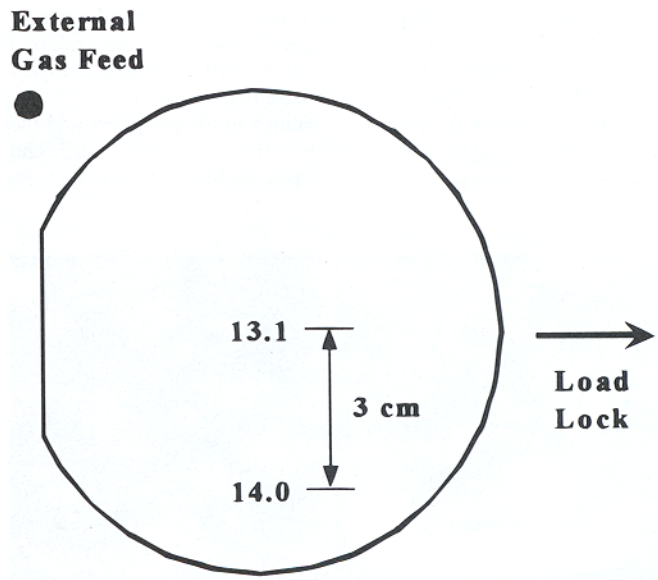

Figure 19. Measured etching depth with the following operating conditions: 140 sccm of SF_6 (10 s active cycle, no overlap, and 8 W electrode power), 20 sccm of C_4F_8 (6 s of active cycle and 6 W electrode power), the APC positioned at 50°. The maximum depth is observed opposite to the location of the external gas feed.

S0013-4651(98)01-009-X CCC: $7.00 © The Electrochemical Society, Inc.

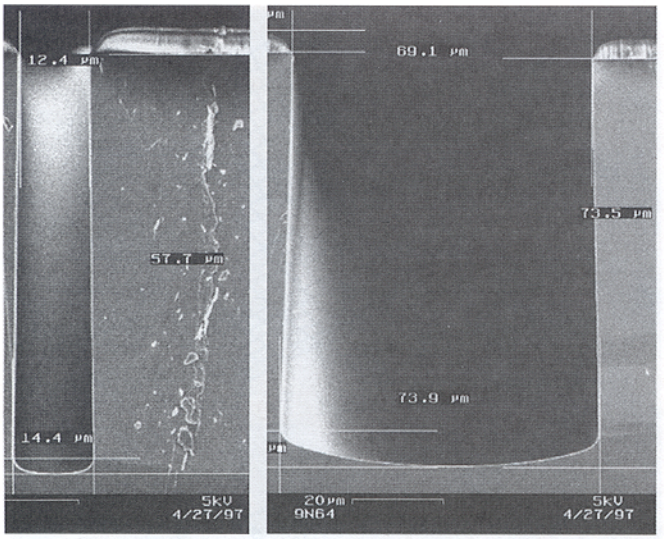

Figure 20. Profile of trenches etched with the operating conditions specified in Fig. 19.

arrangement of the coil power coupling and the gas feed schemes used. Other variables such as temperature uniformity across the wafer, local rates of plasma density loss and formation, and exposed area as well as feature density also play an important role in determining etching uniformity. However, we can significantly simplify this picture focusing on plasma formation. Thus, the plasma density being higher at points closer to the rf power coil, promotes local increases in the etch rate. Therefore, for most operating conditions the etch rate will be higher on the periphery of the wafer. Furthermore, the uneven introduction and pumping of the gases[39] can also promote nonuniformities (Fig. 3).

Uniformity benefits from lower SF_6 flow rates for all power settings in the mid to high applied electrode power regimes (Fig. 18). This is due to the pressure variation with changes in flow rates for a particular position of the APC. Lower pressures improve uniformity[42] because the diffusivity varies inversely with the pressure. Greater diffusivities reduce the plasma nonuniformity providing a better distribution of the ion flux to the wafer. The diffusive gas transport of the neutral reactants is also increased reducing concentration gradients in the gas phase and producing a more uniform neutral flux on the surface. However, larger SF_6 flow rates are preferred for higher etch rates and also to minimize ARDE. Thus a compromise will always be required for all these responses.

Figure 21 shows the profile of features in the periphery and the middle of the wafer with a nonuniformity of 4.8% (56.7 and 54.1 μm). Etching conditions were: 70 sccm SF_6 (10 s active cycle,

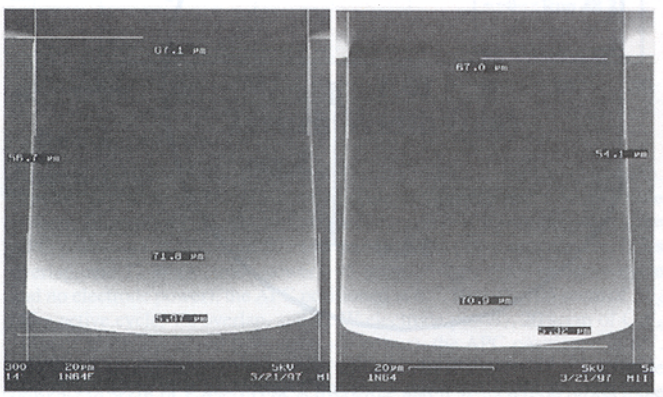

Figure 21. Profile of trenches of nominal width 64 μm. The measured depths for features on the edge of the wafer (left) and in the middle (right) were 56.7 and 54.1 μm, respectively.

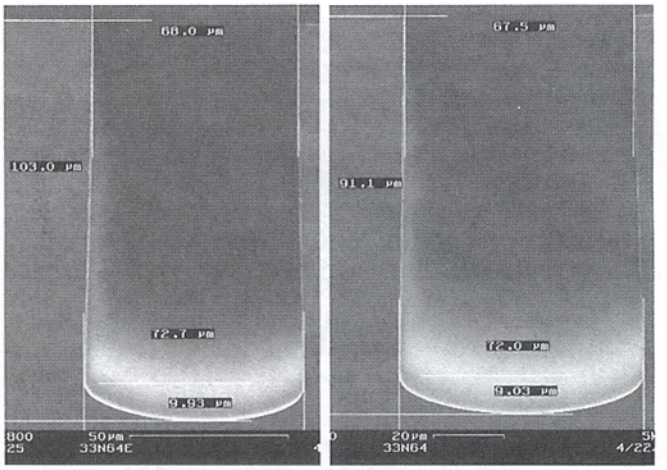

Figure 22. Profile of trenches of nominal width 64 μm. The measured depths for features on the edge of the wafer (left) and in the middle (right), were 103 and 91.1 μm, respectively.

0 s overlap, 8 W electrode power), 20 sccm of C_4F_8 (6 s active cycle, 0 W electrode power), and the APC positioned at 50°. In this case the uniformity is low at the expense of the average etching rate which is only 1.89 μm/min. Inversely, it is also possible to significantly increase the etching rate at the expense of uniformity as is shown in Fig. 22. In this case the etching conditions were: 140 sccm SF_6 (10 s active cycle, 0 sec overlap, 16 W electrode power), 20 sccm of C_4F_8 (6 s active cycle, 3 W electrode power), and the APC positioned at 65°. The measured uniformity is 13.1% and the average etch rate in the middle of the wafer is 3.04 μm/min.

Anisotropy parameter.—This response is of importance in every application, and the ability to tailor the slope of trench walls is one of the more important characteristics of this deep silicon etching tool. The dimensionless anisotropy parameter, α, is defined as the ratio of the trench depth, *h-c*, to the absolute value of the difference

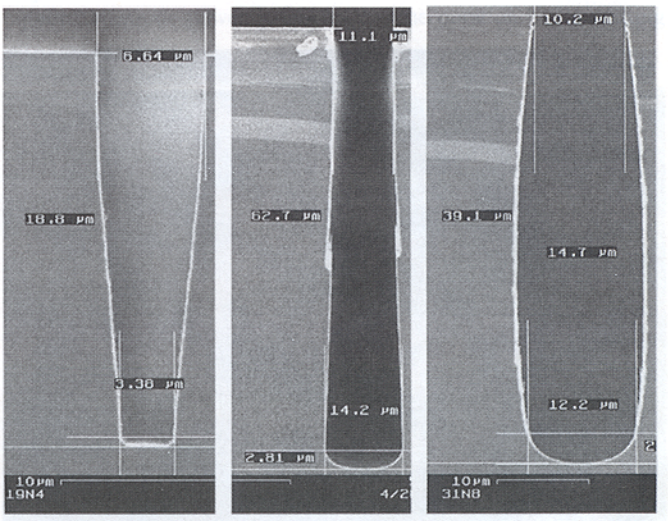

Figure 23. Micrographs showing different profiles obtainable. In (a) the positive slope was achieved with 70 sccm of SF_6 (10 s active cycle, 1 s overlap, and 8 W electrode power), 95 sccm of C_4F_8 (11 s of active cycle, and 6 W electrode power), the APC positioned at 50°. In (b) the etching conditions were 140 sccm of SF_6 (15 s active cycle, 1 s overlap, and 16 W electrode power), 20 sccm of C_4F_8 (6 s of active cycle and 6 W electrode power), the APC positioned at 50°. In (c.) the operating conditions were 70 sccm of SF_6 (12.5 s active cycle, no overlap, and 16 W electrode power), 20 sccm of C_4F_8 (6 s of active cycle and no electrode power), the APC positioned at 80°.

S0013-4651(98)01-009-X CCC: $7.00

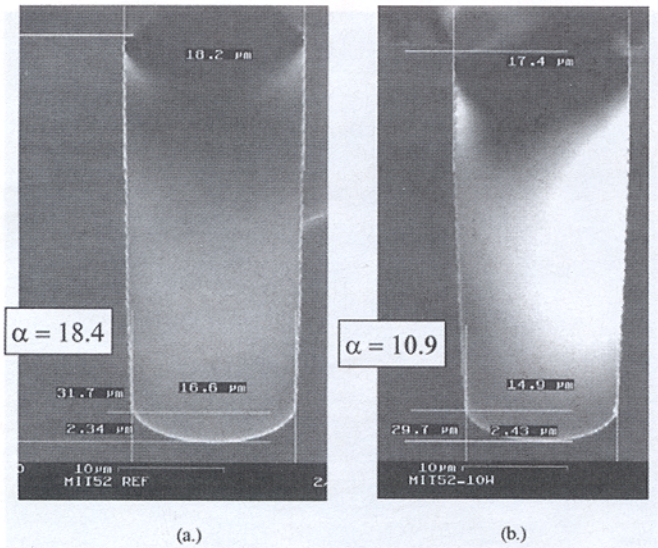

(a.) (b.)

Figure 24. Micrographs showing the effect of lowering the applied electrode power during the etching cycle: from 12 W in (a) to 10 W in (b).

in width at the top compared to that at a reference point at the bottom of the trench, i.e., $(h\text{-}c)/|a\text{-}b|$. The reference point is defined as that where the slope of the wall changes from a straight line to a curved line (see Fig. 4). In most cases, this is easily identifiable (Fig. 23a and b). However, under certain conditions profiles with features not shown in Fig. 4 were observed. Bowing (Fig. 23c) and surface damage (Fig. 17) are cases in point. For these examples, the value considered for anisotropy is the observable general trend of the etching, i.e., reentrant in Fig. 23c, positive in Fig. 17. Choosing the reference point in these cases is arbitrary and makes the predictions of the model inaccurate. Thus, for this particular response, the graphs obtained are qualitative in nature and are not included in this publication. There are, however, a number of observations that must be pointed out. Anisotropy has a well-defined dependence on applied electrode power and chamber pressure.[41] In fact, anisotropy increases as the applied electrode power is increased and an example is shown in Fig. 24, where the power in Fig. 24a is 2 W more than the applied electrode power in Fig. 24b.

With pressure the behavior of this response is different. Initially anisotropy increases with pressure increases, as thicker polymer films

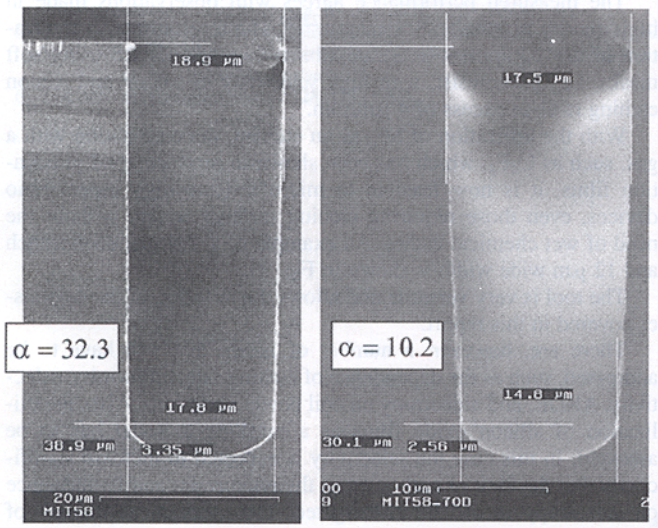

(a.) (b.)

Figure 25. Micrographs showing the effect of increasing the position of the APC valve from 65° in (a) to 70° in (b).

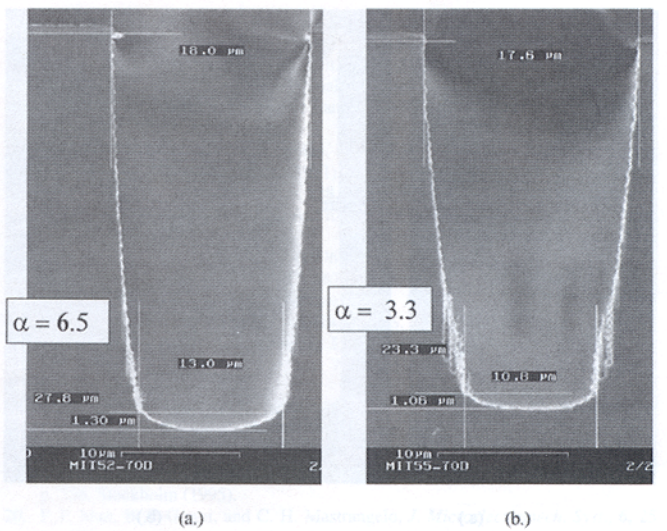

(a.) (b.)

Figure 26. Micrographs showing the effect of increasing the SF_6 flow rate from 105 sccm in (a) to 125 sccm in (b).

are deposited protecting the sidewalls. However, as the pressure is increased even further, the reduction in the average ion energy as well as the increase in the ion angle of incidence[42] combine to produce deleterious effects on anisotropy. Figure 25 shows the anisotropy deterioration as the APC position is increased from 65 to 70°.

It was also observed the relevance of SF_6 flow rate in tailoring the anisotropy: lower SF_6 flow rates are beneficial in producing anisotropic profiles, as can be seen in Fig. 26.

In general, the combination of ion bombardment in conjunction with the formation and preservation of protective films on the sidewalls, allow us to achieve prescribed anisotropy and selectivity targets.[43] Although these protective layers help achieve anisotropic etches, they can be a source of contamination. Oxygen plasmas have been shown to remove them on unpatterned wafers but not on feature sidewalls. This is due to the much reduced ion flux on those walls.

It was generally observed that the anisotropic parameter is larger for 8 μm features compared to 64 μm features, with larger trenches

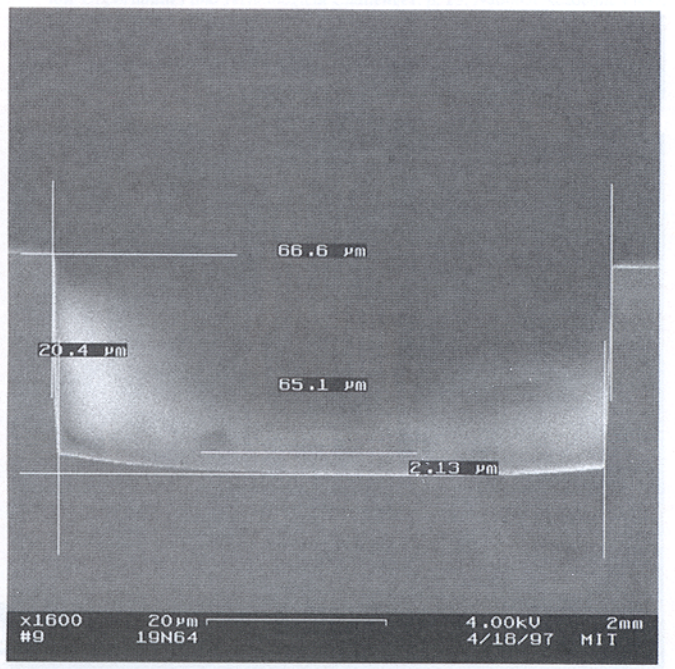

Figure 27. Trench of nominal width 64 μm with a slope significantly less positive than that presented in Fig. 23a for the same etching conditions.

Journal of The Electrochemical Society, **146** (1) 339-349 (1999)
S0013-4651(98)01-009-X CCC: $7.00 © The Electrochemical Society, Inc.

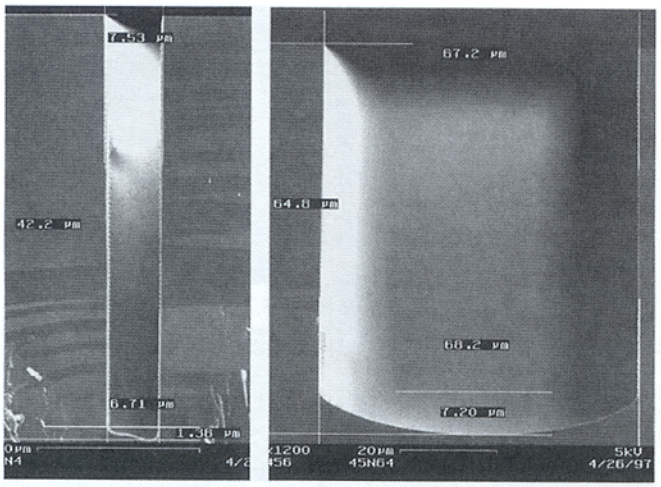

(a.) (b.)

Figure 28. Micrographs showing trenches with a positive slope in (a) and reentrant walls in (b) for the same operating conditions.

tending to become more reentrant, or with a slope less positive. Figures 27 and 23a are a typical case illustrating this point. Thus, it is possible for trenches of dissimilar width to have sloped walls that are positive in one case and negative in the other (Fig. 28).

In addition to high anisotropy, good quality etched features are expected to exhibit no surface damage and no grass. Surface damage can be explained in terms of the polymer films failing and permitting the exposure to plasma to produce uneven and rough surfaces. Figure 17 is a typical example of this effect. During this experiment, it was observed that surface damage was always associated with high APC positions or with passivating active cycles having a similar duration than the etching active cycles.

Grass is formed as masking material is redeposited on flat surfaces creating micromasking sites (see Fig. 29). In addition to high APC settings, high SF_6 flow rates also promote the appearance of grass.

Besides the scalloping previously mentioned, etched walls also have a roughening band extending from the photoresist interface to a depth determined by the operating conditions and the length of time the sample is exposed to plasma etching (see Fig. 30). The origin of this feature is the plasma damage to the photoresist mask, and the subsequent transfer to the walls of the etched topography. It has been reported that the addition of a thin layer of silicon oxide[18] drastically reduces the height of this band.

The presence of vertical striations on etched walls can also be observed in Fig. 30. This effect is due to the photoresist receding unevenly as the etch proceeds. Yet, it is possible to obtain very smooth walls. Such is the case of the operating conditions specified in Fig. 11.

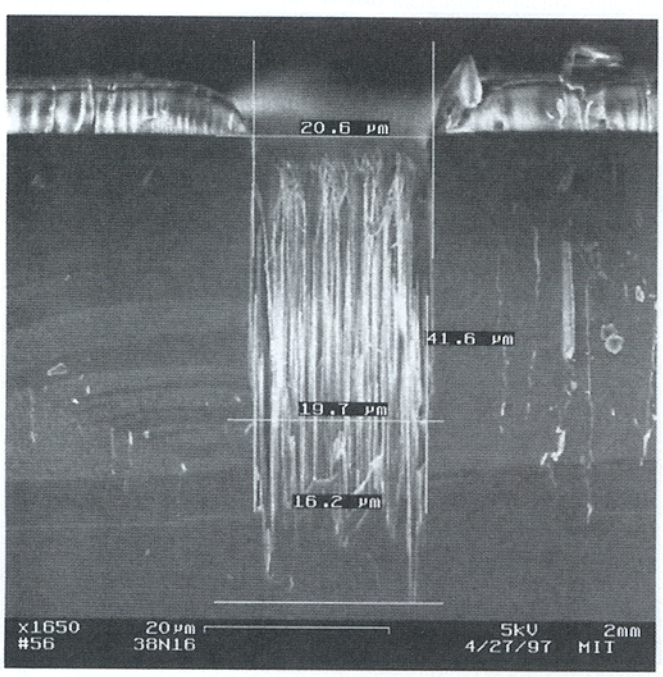

Figure 29. Trench etched with the APC positioned at 65° but with an SF_6 flow rate of 140 sccm.

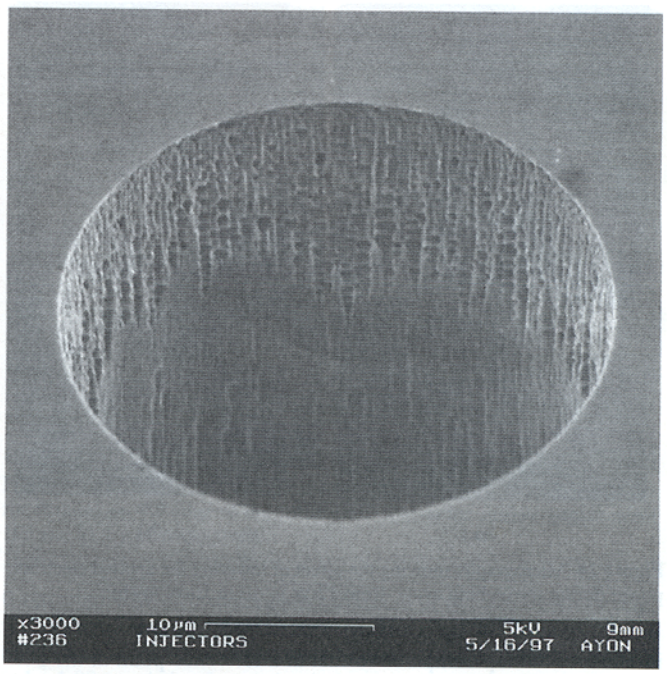

Figure 30. Micrograph showing the roughening band at the top of a 35 μm hole etched through a double-side polished, 450 μm thick silicon wafer.

Conclusion

We have characterized the response dependence of etch rate, ARDE, photoresist etch rate, uniformity and anisotropy, on etching conditions for a time multiplexed inductively coupled plasma etcher.

The measured performance agrees with observations made in high density plasma environments.[22,30] The most attractive innovation of this equipment is the possibility to attain HARS using soft masks, i.e., photoresist, with high selectivity to silicon and silicon etching rates in excess of 4 μm/min.

With the utilization of SF_6 as an etchant, in combination with a gas, such as C_4F_8, which has been shown to produce good passivation films, it is now feasible to microfabricate high aspect ratio devices, even those requiring etching through wafers without the need of wet chemical etches. An example of a 404 μm deep trench and 12 μm wide width is shown in Fig. 31.

The tool is very versatile and allows the tailoring of the responses covered in this report.

There are, however, a number of issues that still have to be addressed, such as the dependence of etching rate, uniformity, selectivity, ARDE, and anisotropy on coil power variations. Also, the utilization of silicon oxide films as a masking material has to be assessed. In this case the selectivity is expected to increase significantly, but the lack of carbon from the photoresist and its influence on anisotropy should be investigated. The mechanical strength of etched samples depends on the radius of curvature of the feature bottom (see Fig. 5), which in turn is determined by etching conditions. Thus, the measured strength of silicon biaxial samples also has to be investigated.

S0013-4651(98)01-009-X CCC: $7.00

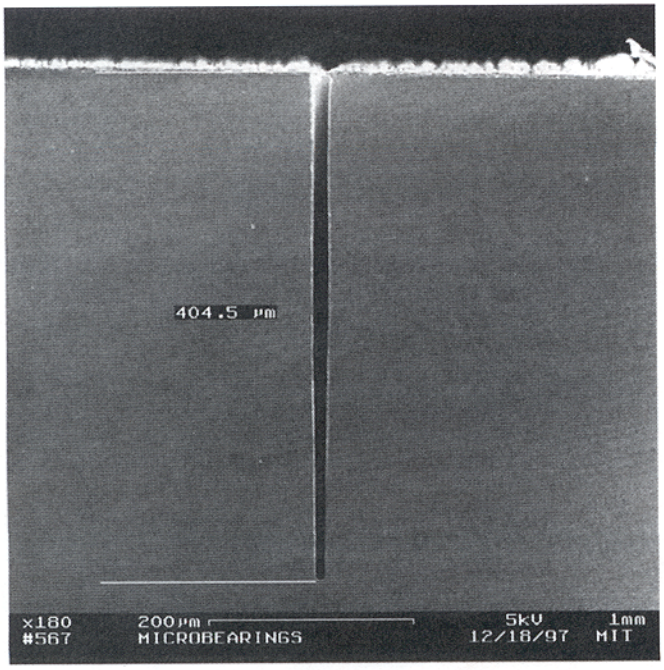

Figure 31. A trench 12 µm wide and 404 µm deep etched with the tool described herein.

Acknowledgments

We thank Dr. R. Paur, Technical Manager of the U.S. Army Research Office, and Dr. R. Nowak, Program Manager of DARPA, for the financial support provided for this project, and a NSF Fellowship (R.A.B.). The cooperation of the staff of the Microsystems Technology Laboratories at MIT is also appreciated.

Massachusetts Institute of Technology assisted in meeting the publication costs of this article.

References

1. E. H. Klaasen, K. Petersen, J. M. Noworolski, J. Logan, N. I. Maluf, J. Brown, C. Storment, W. McCulley, and G. T. A. Kovacs, in *Proceedings of Transducers '95*, p. 556, Stockholm (1995).
2. A. H. Epstein and S. D. Senturia, *Science*, **276,** 1211 (1997).
3. P. J. Hesketh and J. D. Harrison, *The Electrochemical Society, Interface*, **3**(4) (1994).
4. W. Ehrfeld, P. Bley, F. Gotz, P. Hagmann, A. Maner, J. Mohr, H. O. Moser, D. Munchmeyer, D. Schmidt, and E. W. Becker, in *Proceedings of the IEEE Micro Robots and Teleoperators Workshop*, Hyannis, MA, IEEE (1987).
5. E. H. Evans, J. J. Giglio, T. M. Castillano, and J. Caruso, *Inductively Coupled and Microwave Induced Plasma Sources for Mass Spectrometry*, p. 7, The Royal Society of Chemistry, Cambridge, England (1995).
6. J. A. Mucha, *Solid State Technol.*, **28,** 123 (1985).
7. R. d'Agostino and D. L. Flamm, *J. Appl. Phys.*, **52,** 162 (1981).
8. Y. Tzeng and T. H. Lin, *J. Electrochem. Soc.*, **134,** 2304 (1987).
9. C. P. D'Emic, K. K. Chan, and J. Blum, *J. Vac. Sci. Technol. B*, **10,** 1105 (1992).
10. T. Syau, B. J. Baligam, and R. W. Hamaker, *J. Electrochem. Soc.*, **138,** 3076 (1992).
11. Robert Bosch GmbH, Pat. 4,855,017 and 4,784,720 (USA) and 4241045C1 (Germany) (1994).
12. A. J. Roosmalen, J. A. G. Baggerman, and S. J. H. Brader, *Dry Etching for VLSI*, p. 113, Plenum Press, New York (1991).
13. K. M. Eisele, *J. Electrochem. Soc.*, **128,** 123 (1981).
14. D. L. Flammm D. E. Ibbotson, J. A. Mucha, and V. M. Donnelly, *Solid State Technol.*, **26,** 117 (1983).
15. P. Singer, *Semicond. Int.*, **19,** 152 (1996).
16. S. Matsuo, *J. Vac. Sci. Technol.*, **17,** 587 (1980).
17. A. Epstein, S. D. Senturia, G. Anathasuresh, A. Ayon, K. Breuer, K-S Chen, F. E. Ehrich, G. Gauba, R. Ghodssi, C. Groshenry, S. Jacobson, J. H. Lang, C.-C. Lin, A. Mehra, J. M. Miranda, S. Nagle, D. J. Orr, E. Piekos, M. A. Schmidt, G. Shirley, M. S, Spearing, C. S. Tan, and I. A. Waitz, in *Proceedings of Transducers '97*, Chicago, IL (1997).
18. R. Bayt, A. A. Ayon, and K. Breuer, Paper presented at 33rd AIAA/ASME/SAE/ASEE Joint Propulsion Conference and Exhibit, Seattle, WA (1997).
19. E. H. Klaasen, K. Petersen, J. M. Noworolski, J. Logan, N. I. Maluf, J. Brown, C. Storment, W. McCulley, and G. T. A. Kovacs, in *Proceedings of Transducers '95*, p. 556, Stockholm (1995).
20. P. F. Man, B. P. Gogoi, and C. H. Mastrangelo, *J. Microelectromech. Syst.*, **6,** 25 (1997).
21. G. M. Whitesides, in *Proceedings of Transducers '97*, p. 23, Chicago, IL (1997).
22. C. Lee, D. B. Graves, and M. A. Lieberman, *Plasma Chem. Plasma Proc.*, **16,** 1 (1996).
23. I. Tepermeister, N. Blayo, F. P. Klemens, D. E. Ibbotson, R. A. Gottscho, J. T. C. Lee, and H. H. Sawin, *J. Vac. Sci. Technol. B*, **12,** 2310 (1994).
24. G. S. Oehrlein and R. F. Rembetski, *IBM J. Res. Develop.*, **36,** 140 (1992).
25. K. D. Allen, H. H. Sawin, and A. Yokozeki, *J. Electrochem. Soc.*, **133,** 2331 (1986).
26. D. Mannos and D. Flamm, *Plasma Etching*, p. 101, Academic Press, New York (1989).
27. U. S. Tandon and B. D. Pant, *Vacuum*, **42,** 837 (1991).
28. R. J. Schutz, in *VLSI Technol.*, 2nd ed., S. M. Sze, Editor, p. 206, McGraw-Hill, New York (1988).
29. D. Bollinger, S. Lida, and O. Matsumoto, *Solid State Technol.*, **27,** 111 (1984).
30. D. C. Gray, I. Tepermeister, and H. H. Sawin, *J. Vac. Sci. Technol. B*, **11,** 1243 (1993).
31. D. C. Gray, Ph.D. Thesis, Massachusetts Institute of Technology, Cambridge, MA (1992).
32. D. C. Gray, J. W. Butterbaugh, and H. H. Sawin, *J. Vac. Sci. Technol., A*, **9,** 779 (1991).
33. T. J. Dalton and H. H. Sawin, Paper presented at 41st Symposium of the American Vacuum Society, Denver, CO (1994).
34. T. J. Dalton, Ph.D. Thesis, Massachusetts Institute of Technology, Cambridge, MA (1994).
35. R. A. Gottscho, C. W. Jurgensen, and D. J. Vitkavage, *J. Vac. Sci. Technol. B*, **10,** 2133 (1992).
36. D. Chin, S. H. Dhong, and G. J. Long, *J. Electrochem. Soc.*, **132,** 1705 (1985).
37. Panel on Plasma Processing of Materials, *Plasma Processing of Materials: Scientific Opportunities and Technological Challenges*, p. 23, National Academic Press, New York (1991).
38. G. S. Oehrlein, J. F. Rembetski, and E. H. Payne, *J. Vac. Sci. Technol. B*, **8,** 1199 (1990).
39. A. Grill, *Cold Plasma in Materials Fabrication*, p. 97, IEEE Press, New York (1994).
40. M. Pichot, *Vacuum*, **41,** 895 (1990).
41. C. B. Zarowin, *J. Vac. Sci. Technol. A*, **2,** 1537 (1984).
42. J. Liu, G. L. Huppert, and H. H. Sawin, *J. Appl. Phys.*, **68,** 3916 (1990).
43. P. H. Singer, *Semicond. Inter.*, **11,** 68 (1988).

Reprinted from JOURNAL OF THE ELECTROCHEMICAL SOCIETY
Vol. 146, No. 1, January 1999
Printed in U.S.A.